Mars Sample Return Earth Entry System Helicopter Drop Test Reconstruction

Christopher D. Karlgaard*
Analytical Mechanics Associates, Inc., Hampton, VA, 23666

Rohan G. Deshmukh†, Mark Schoenenberger‡
NASA Langley Research Center, Hampton, VA, 23681

Michael S. Manwell§
Analytical Mechanics Associates, Inc., Hampton, VA, 23666

James M. Corliss¶
Corliss Consulting LLC, Williamsburg, VA, 23185

The Mars Sample Return campaign conducted four successful helicopter drop tests of the Earth Entry System at the Utah Test and Training Range on October, 2023. The tests acquired data for the 52.5 deg sphere cone geometry that can be used to develop models for the terminal descent aerodynamics and flight dynamics used to model ground impact conditions. The acquired test data included both sensor data outputs from an on-board inertial measurement unit, global positioning system, and video cameras as well as atmospheric measurements from weather balloons. This data was processed using a Kalman filter/smoother to reconstruct the capsule's trajectory and aerodynamics. An equation-error method was used to reconcile the aerodynamics by solving for a set of dispersions in the aerodynamic database that form a best-fit to the reconstructed aerodynamics. The reconstructed trajectories were compared with flight simulations generated using Program to Optimize Simulated Trajectories II. The results indicate that the simulation underpredicted the vehicle oscillation amplitudes. The reconstruction exhibits a persistent low-amplitude oscillation that does not damp out as predicted.

Nomenclature

C_A	=	Axial force coefficient
C_l	=	Rolling moment coefficient
C_m	=	Pitching moment coefficient
C_N	=	Normal force coefficient
C_n	=	Yawing moment coefficient
C_Y	=	Side force coefficient
h_{agl}	=	Above ground level altitude, m
I_{xx}, I_{yy}, I_{zz}	=	Principal moments of inertia, kg-m^2
m	=	Mass, kg
t_f	=	Flight time, s
V	=	Magnitude of North-East-Down velocity, m/s
V_H	=	Apparent wind, m/s
V_n, V_e, V_d	=	North-East-Down velocity components, m/s
V_x, V_y, V_z	=	Body velocity components, m/s
V_∞	=	Wind-relative velocity magnitude, m/s

*Aerospace Engineer, Associate Fellow AIAA.
†Aerospace Engineer Atmospheric Flight and Entry Systems Branch, Senior Member AIAA.
‡Aerospace Engineer, Atmospheric Flight and Entry Systems Branch, Senior Member AIAA.
§Aerospace Engineer.
¶Aerospace engineer.

x_{cm}, y_{cm}, z_{cm} = Components of the center of mass location relative to nose, m
α = Angle of attack, rad
α_0 = Initial angle of attack, rad
α_T = Total angle of attack, rad
β = Angle of sideslip, rad
ϕ, θ, ψ = Roll, pitch, and yaw Euler angles, rad
Ω = Magnitude of angular velocity, rad/s
$\omega_x, \omega_y, \omega_z$ = Body axis angular velocity componets, rad/s

I. Introduction

The Mars Sample Return (MSR) Earth Entry System (EES) [1] is a passive entry capsule developed by the National Aeronautics and Space Administration (NASA) to return Mars soil and rock samples back to Earth. While the MSR campaign is currently undergoing a re-architecture, the work presented in this paper is based on an December 2023 MSR architecture. The EES is planned to land without a parachute at the Utah Test and Training Range (UTTR). Because the EES does not rely on a parachute to decelerate, the capsule will impact the ground at UTTR with velocities up to 45 m/s (100 mph). It is critical that the capsule structure is designed such that the loads imparted on the Mars samples do not exceed acceptable limits. Meeting these requirements depends on: 1) the soil properties in the intended UTTR landing area, 2) the structural response of the EES aeroshell, 3) the ability of computational models to predict the capsule's response when impacting the soil, and 4) the ability of computational models to predict the capsule's ground impact conditions. This paper focuses on 4) where computational models are utilized to reconstruct the trajectory of EES drop tests for prediction of ground impact conditions.

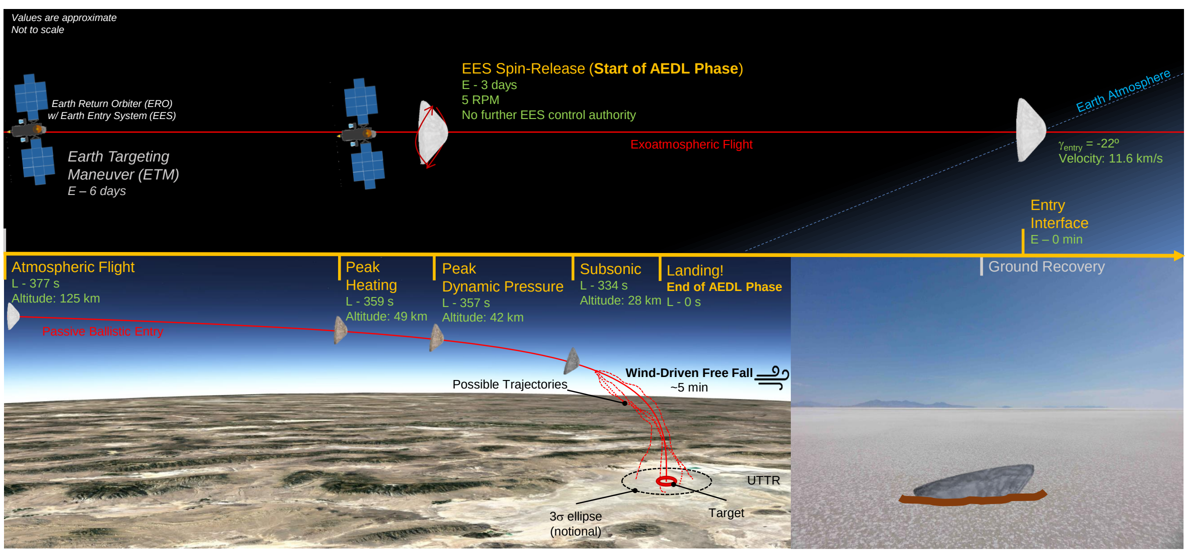

Fig. 1 Notional approach entry, descent, and landing concepts of operations for EES.

Figure 1 illustrates the notional concept of operations for the Approach Entry, Descent, and Landing phase of MSR*. As a passive entry capsule, EES spends about 5 min in terminal free-fall where the main perturbations to trajectory arise from winds in the surrounding UTTR region. Conditions during this portion of the trajectory can be generally replicated via helicopter drop tests. This makes drop tests an important for assessing EES aeroshell attitude dynamics during terminal free-fall and generating flight-like ground-impact conditions for assessment of structural performance.

The MSR EES project has conducted a series of drop test campaigns at UTTR. Previously conducted drop tests were focused on deriving and validating computational soil models used to predict the EES response during ground impact. The test plan included drop tests of penetrometers with 60 deg and 45 deg sphere-cone geometries as well as drop tests of a full-scale 52.5 deg sphere-cone aeroshell. To date, 75 drop tests of these test articles have been conducted at UTTR from November 2019 through April 2023.

*Development of Capture, Containment and Return System (CCRS) portion of MSR is currently paused. Figure is representative of architecture as of CCRS Preliminary Design Review Part 2 December 2023.

In October 2023, the project conducted four successful helicopter drop tests at UTTR. The primary test objective was to acquire the first set of terminal descent flight dynamics data for the 52.5 deg sphere cone EES geometry with flight-like mass properties. These data will contribute to anchoring the aerodynamics and flight dynamics models used to predict the EES terminal descent behavior and landing conditions. A secondary test objective was to acquire the first set of ground impact data for the 52.5 deg sphere-cone capsule configuration.

II. Test Article

The test article was a full-scale representation of the EES flight vehicle outer mold line (OML) geometry and mass properties. The basic test article geometry is a 52.5-deg sphere-cone shape with a 1.273 m diameter and 0.3146 m nose radius. The primary sphere-cone structure was fabricated from two pieces of machined aluminum fastened together, with additional machined aluminum components that form the aft body lid and the lid's support structure. The backshell conical geometry is formed by six fiberglass-covered foam segments, and the backshell aft deck is constructed of a carbon graphite composite panel. Three lifting brackets are secured around the test article periphery to which lifting straps are attached to suspend the test article from the helicopter release hook. The test article was structurally designed to withstand ground impacts into the UTTR soil with impact angles up to 15 degrees.

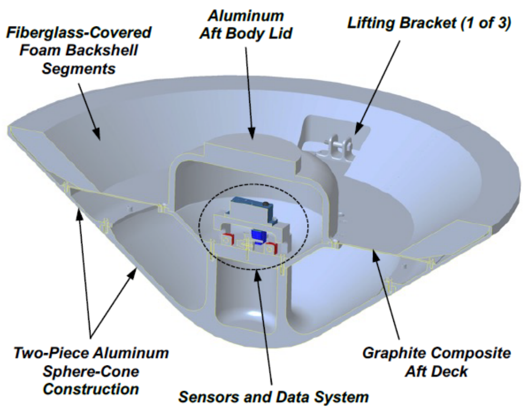

(a) Design configuration.

(b) As-built test article.

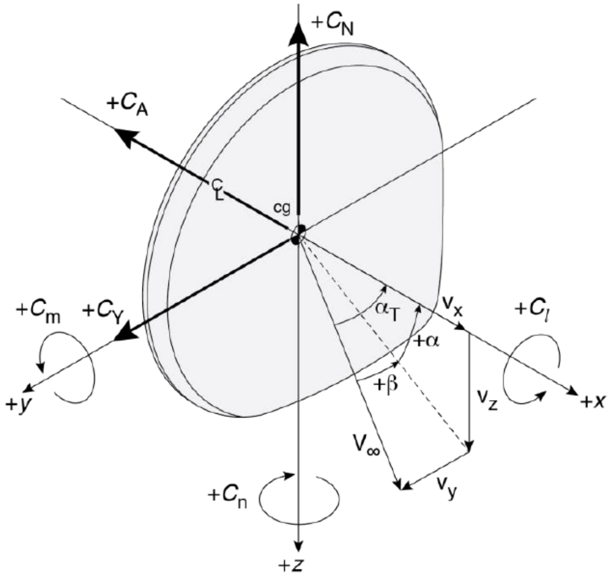

(c) Aerodynamic coordinate frame.

Fig. 2 EES drop test article.

The test vehicle aerodynamic coordinate system is shown in Fig. 2(c). This figure shows the definitions of the aerodynamic flow angles and the aerodynamic force and moment directions. Additional detail on the vehicle aerodynamics is given in Sec. IV.E.

III. Test Operations

Each drop test is conducted using a helicopter where lifting straps are used to connect the helicopter drop hook to the capsule. Prior to being lifted into the air, the capsule's data acquisition system is "zeroed" on the ground. This sets the reference for the IMU acceleration and rate measurements.The helicopter lifts off with the capsule and ascends to the prescribed drop altitude. Unlike previous drop test conducted, a novel release methodology is developed.

The tests were conducted using a "Perturbation Drop Testing" technique, illustrated in Fig. 3, to force the EES test article into varying magnitudes of oscillatory motion immediately after being released from the helicopter. Perturbing the test article initial attitude and attitude rates in this manner enabled the team to measure the vehicle's aerodynamic stability characteristics and stress the EES flight dynamics models.

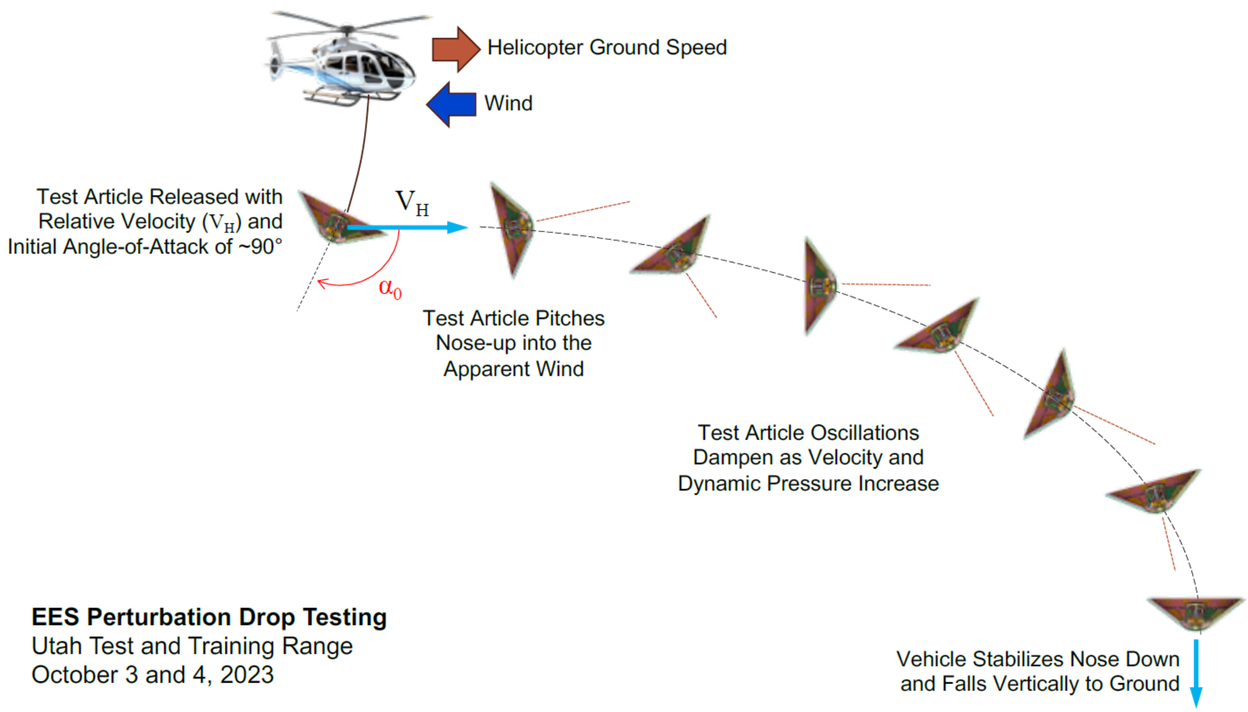

Fig. 3 Helicopter drop test concept of operations. Image exaggerated for visual clarity.

The magnitude of the initial perturbation to the test article was varied by adjusting the relative horizontal velocity, or "Apparent Wind" (V_H) between the test article and the atmosphere. The apparent wind produces an aerodynamic pitching moment on the capsule while it is suspended beneath the helicopter. When the test article is released from the helicopter, it immediately rotates with a pitch rate dictated by the magnitude of the pitching moment and the test article mass properties. As the test article proceeds through the trajectory and dynamic pressure increases, the vehicle's aerodynamics dampen the initial pitching oscillations and the capsule orients itself nose down, falling nearly vertically to the ground. The goal of this drop test campaign was to produce a set of flight dynamics data that captured the EES performance across a wide range of initial pitch rate perturbations.

Adjusting the test article pitch rate perturbation required knowledge of the winds at the release altitude and the ability to control the helicopter heading and ground speed. Maintaining a relatively low ground speed is a challenging aspect of these tests, as the helicopter pilot is constantly adjusting the controls to compensate for winds while simultaneously working to limit the pendulum motion of the test article suspended beneath the helicopter. The winds aloft were measured immediately before each drop test using a weather balloon launched at the test site by the Dugway Meteorological Office. The test team used the wind data to select a testing altitude and to establish a helicopter heading and ground speed to produce the desired apparent wind and intended pitch rate perturbation for the test. These test conditions were guided by pre-test simulations [2] and quick-look data from preceding tests that enabled the team to roughly correlate the apparent wind to the test article pitch rate.

Table 1 Drop test matrix.

Drop Test	h_{agl} m	V m/s	Ω deg/s	t_f s
1	1623.8	20.0	22.7	40.252
2	1195.8	7.2	7.8	30.906
3	1567.6	3.2	6.4	38.932
4	1588.6	8.3	4.3	40.008

Fig. 4 Test article during drop.

Four drop tests were successfully completed on October 3 and 4 using this testing process. A summary of the GPS measured altitude, velocity, and impact times of the four drop tests are summarized in Table 1. These four tests produced initial pitch rate perturbations across the desired range of interest. In all four tests the vehicle's inherent aerodynamic stability damped out the initial dynamics and the test article descended to the ground exhibiting very stable flight with low-amplitude oscillatory motion. The vehicle repeatedly landed on its nose and produced ground impact accelerations consistent with pre-test predictions. Fig. 4 show the EES test article at various points throughout a drop test sequence as it is released from the helicopter and descends to the ground. All flight dynamics measurements, ground impact measurements, GPS data, and test video were successfully acquired for these tests, thereby meeting the success criteria of the primary and secondary objectives of the test campaign.

IV. Data Sources

The data sources available for the reconstruction include weather balloons, Inertial Measurement Unit (IMU) data that includes three-axis linear accelerations and angular rates, GPS position and velocity measurements, and video data.

A. Inertial Measurement Unit

The IMU was a Texense IB6 device that recorded accelerations and angular rates at a sample rate of 50 kHz. The IMU data were filtered and downsampled to a rate of 500 Hz for trajectory reconstruction. The z-axis angular rates measured in drop test 1 were saturated above the upper limit of 157.4 deg at 4 portions in the trajectory and below the lower limit of -183.65 deg/s at 1 portion, all corresponding to upper and lower peaks of oscillations. Data beyond the saturation limits were reconstructed by estimating coefficients of a second-order polynomial by fitting a portion of data prior to saturation and after de-saturation. An example of the saturated signal and the polynomial extrapolation is shown in Fig, 5. The rate gyros did not saturate during the remaining drop tests.

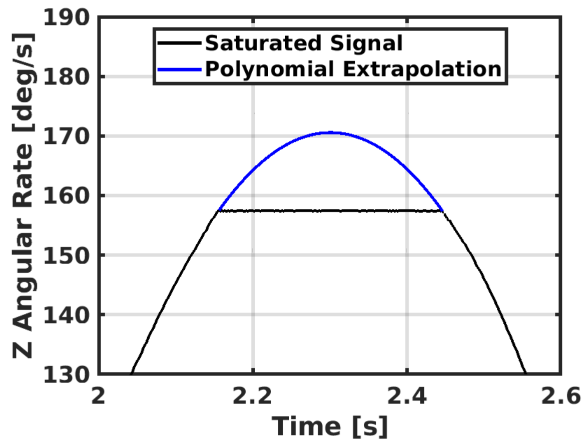

Fig. 5 Drop 1 rate saturation.

The IMU accelerations were transformed from the instrument location to the center of mass as part of the reconstruction process. The lever arm for the calculation was based on the measured location of the installed IMU and the measured mass properties. The linear accelerations and angular rates from the drop tests are shown in Fig. 6. The IMU was calibrated by the vendor. Uncertainties in the data were based on the sensor specification sheets which indicate accuracies within 2% of the full scale range. The body x-axis accelerometer had a full scale range of 5 g's, the y and z-axis accelerometers had a full scale range of 3 g's, and all gyroscopes had a full scale range of 150 deg/s.

Additionally, there were several high-range accelerometers to measure the impact accelerations. These consisted of two Measurement Specialties 3801A 500-g range accelerometers in the lateral directions and a similar unit with a 2000-g range in the axial direction. A second independent measurement of the test article impact accelerations was provided by a Endevco PS7274 3-axis accelerometer with a 20,000 G range in each axis. These high-range sensors were used in conjunction with the reconstructed impact conditions for soil and structural analysis, which is not described in this paper.

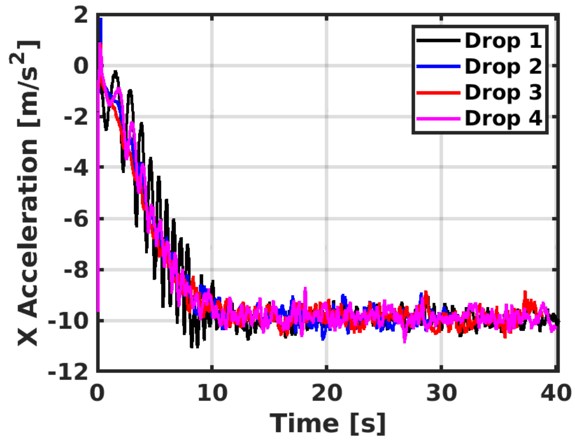

(a) Accelerations.

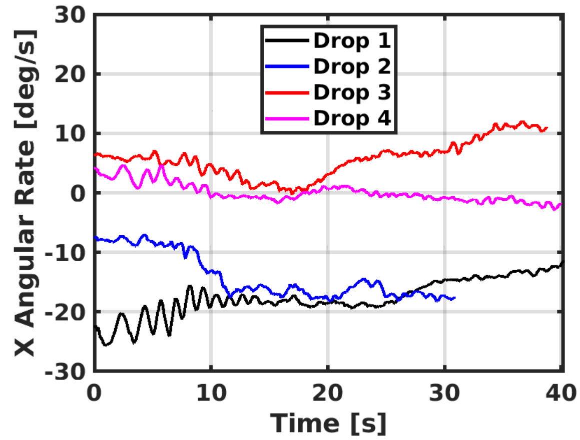

(b) Angular rates.

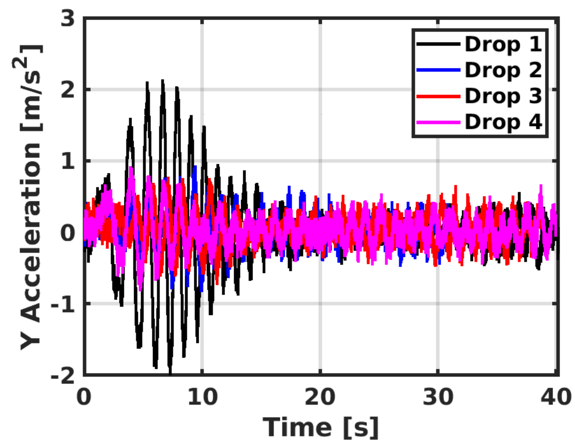

(c) Accelerations.

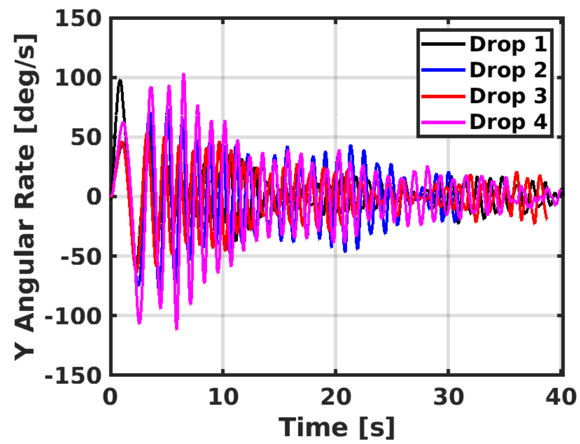

(d) Angular rates.

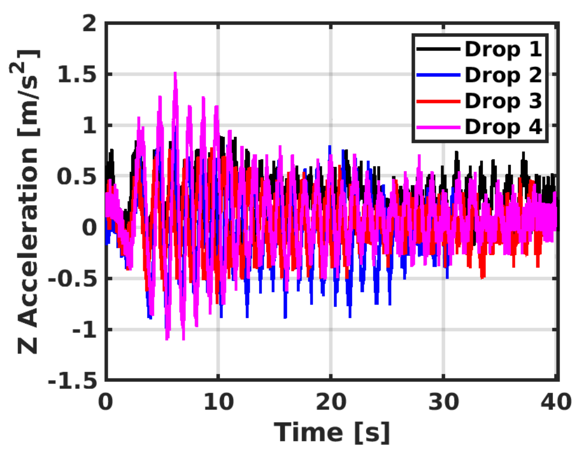

(e) Accelerations.

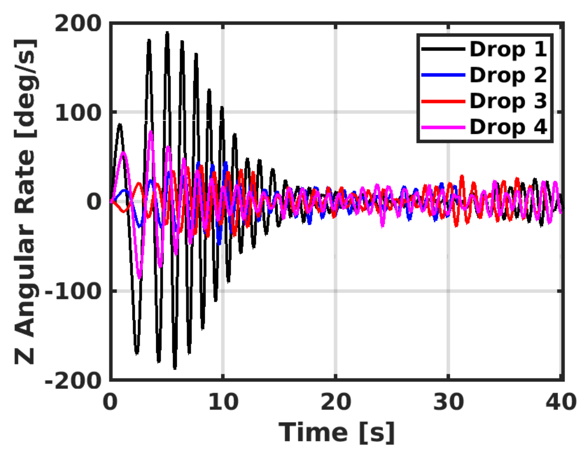

(f) Angular rates.

Fig. 6 IMU data.

B. Global Positioning System

The GPS device was a Flysight unit produced by Bionic Avionics, Inc., that reported geodetic position and North-East-Down (NED) velocity at a sample rate of 5 Hz. Estimates of the accuracy of the position and velocity solutions are also computed by the unit based on the number and geometry of the GPS satellites in view. The Flysight GPS unit was not shock rated. Post-impact data from the unit was not realistic, however within several seconds the signals returned to expected values.

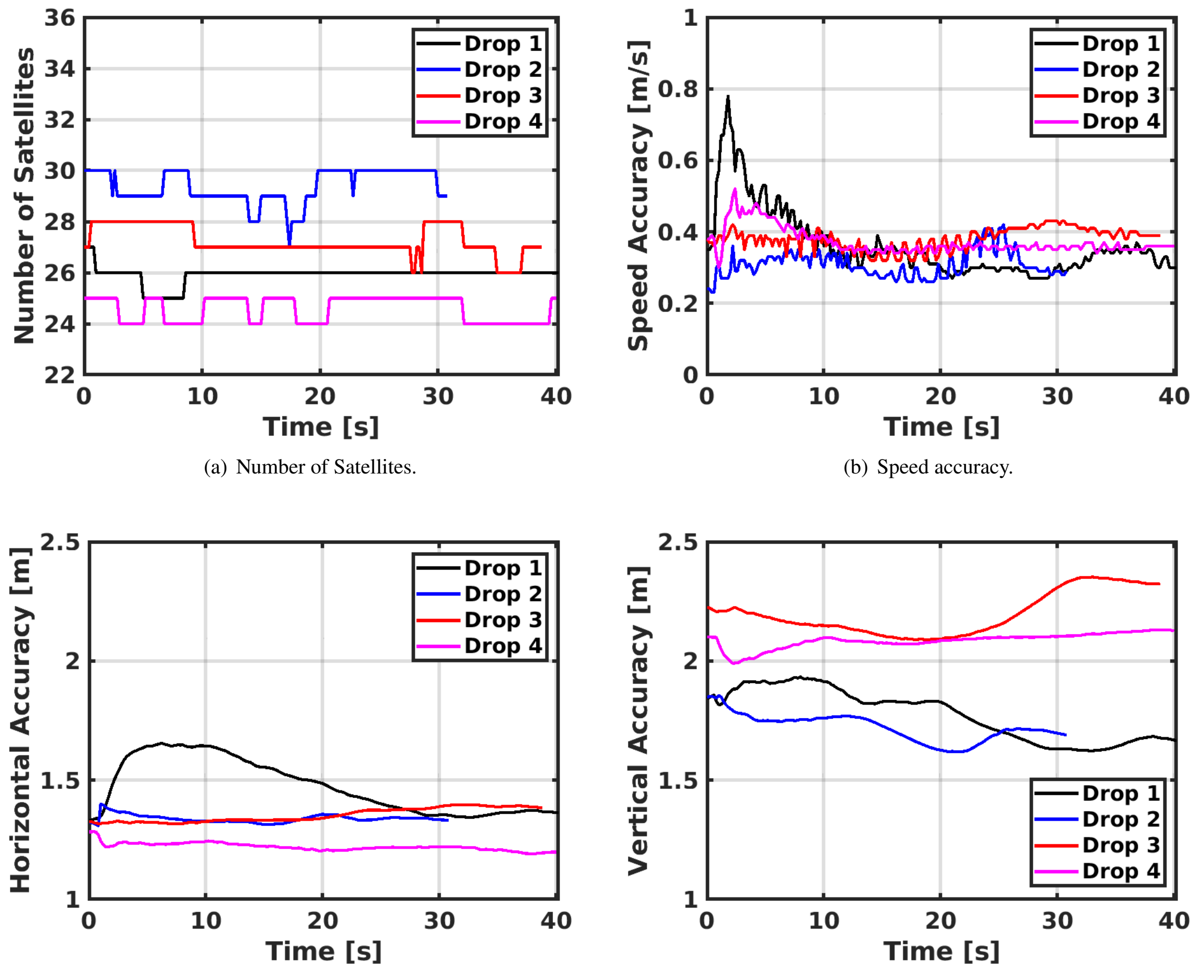

(a) Number of Satellites.

(b) Speed accuracy.

(c) Horizontal accuracy.

(d) Vertical accuracy.

Fig. 7 GPS performance metrics.

GPS performance data are shown in Fig. 7. As shown in Fig. 7(a), each drop test used data from between 24 and 30 satellites in the GPS solution position and velocity solution. The reported speed accuracies are shown in Fig. 7(b). Only a single speed accuracy is reported by the Flysight unit. It was assumed that the speed accuracy values were to be applied as 1σ uncertainties in each component of the computed North-East-Down velocity and that these components were uncorrelated. The Flysight unit reported two components of accuracy in the position solution corresponding to horizontal and vertical positions, shown in Fig. 7(c) and (d), respectively. The horizontal position accuracies were transformed into an equivalent angle applied as 1σ uncertainties in the computed latitude and longitude angles. The vertical accuracy was applied as a 1σ uncertainty in the altitude solution. The position uncertainties were also assumed to be uncorrelated.

C. Video

Four Sony real-time 4k resolution cameras were installed on the test article to record orientation of the ±X and ±Y drop test axes relative to the horizon during the drop test at 30 frames per second. An example still image from drop test 1 at ground impact is shown in Fig. 8. Note that the horizon is visible in the right side of the image indicating an angular offset at the instant of ground impact.Though the videos do not provide measured flight data, they do provide useful qualitative information on the vehicle dynamics.

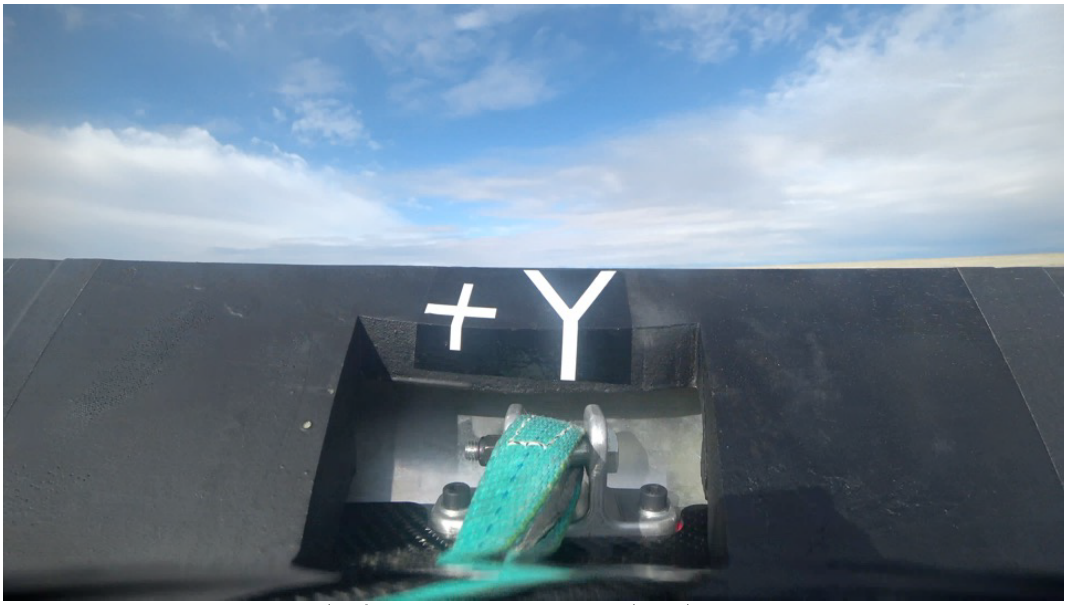

Fig. 8 Example on-board video image.

D. Weather Balloons

Atmospheric conditions were measured by releasing weather balloons to acquire meteorological data from the ground to approximately 20km altitude. A weather balloon was released prior to each test to provide wind data to the test team to determine the appropriate altitude, ground speed, and heading for each test. The meteorological data were also used for the post-flight analysis to determine the atmospheric-relative trajectory.

The meteorological data in the form of north and east wind components, and the density, pressure, and temperature are shown in Fig. 9. Fig. 9(a) and (b) show the north and east components of the winds, Fig. 9(c)–(e) shows the temperature, pressure, and density, respectively. Uncertainties in the meteorological data were assumed to be 1% in pressure and density and 1 m/s in wind velocity, each in a 3σ sense. Fig. 9(f) shows the ratio of the measured density to the Global Reference Atmosphere Model (GRAM)[3] monthly mean value, which is used in the pre-test predictions. The measured density profiles are 1% higher compared to the monthly mean over most of the trajectories.

E. Aerodynamic Database

The aerodynamic database used for pretest predictions and test design, and post-flight reconciliation simulations consists of tables of static and dynamic aerodynamic coefficients for the full range of conditions the flight vehicle will experience during entry (from rarefied flow at entry down to subsonic terminal velocity conditions). The database has internal interpolations routines which return smooth surfaces for each coefficient as a function Mach number and angles of attack and sideslip. For the helicopter drop tests, the velocity never exceeded 45 m/s so the low subsonic data in the aerodatabase was all that was utilized. Data for the terminal velocity phase of the trajectory was measured experimentally in NASA Langley's Transonic Dynamics Tunnel (TDT) and 20 Foot Vertical Spin Tunnel (VST). The data from the EES static and dynamic tests will be published the future. TDT models were 559 mm in diameter and VST models were 35 0mm in diameter. In both tunnels, models were supported by a strut mounted through the side of the forebody at the expected flight center of mass station (0.214 diameters aft of the nose). In TDT, the support spanned the entire test section and was actuated by a motor outside the tunnel. In the VST, the strut was mounted on a sting in the

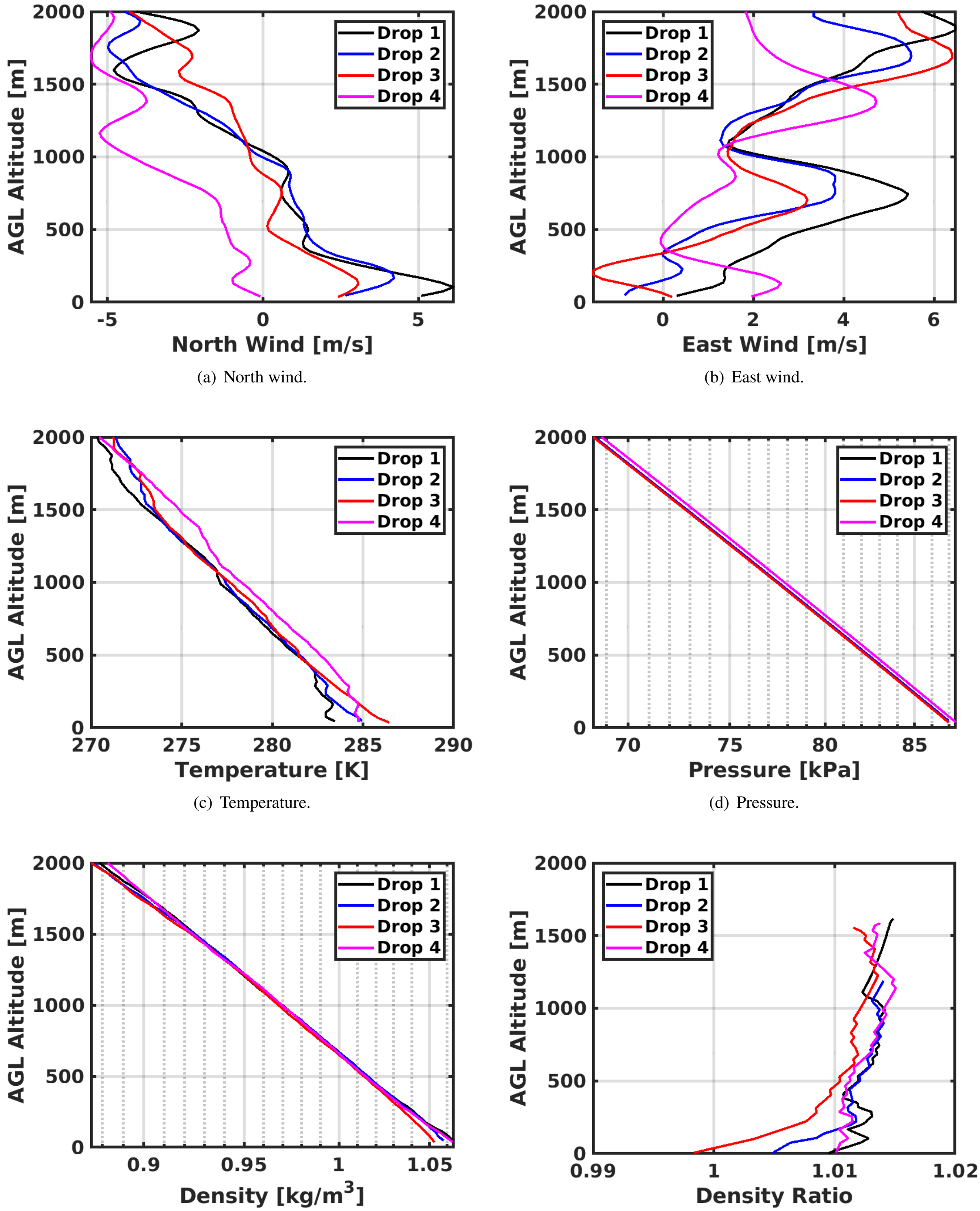

(a) North wind. (b) East wind. (c) Temperature. (d) Pressure. (e) Density. (f) Density ratio.

Fig. 9 Atmosphere data.

tunnel and supported the model from one side only. The strut drive motors were used to sweep the model through a large angle of attack range for static data; For dynamic forced oscillation testing, the strut was rotated to generate sinusoidal pitching motion closely matching the expected flight reduced frequencies. TDT data was collected at Reynolds numbers of 1.0 and 2.33 million (model diameter used as reference length). These test conditions reasonably approximated the drop test conditions (Reynolds numbers of 2.9 million at a terminal velocity of 40 m/s). Uncertainties on the test data were based on repeats runs and comparisons of reflected data (data at mirrored positive and negative angles of attack). These uncertainties are modeled in the aerodatabase. The best fit trajectories shown below identified the deviations from the wind tunnel aerodynamics that best recreate the drop test performance and are compared to the aerodatabase uncertainties.

F. Mass Properties

The test article mass properties were measured at a facility located at NASA Langley Research Center. The measurements included mass, center of mass position, and moments of inertia normal to the axis of symmetry. The moment of inertia about the axis of symmetry was not measured. The design value was used for the reconstruction. The mass properties were measured without the on-board cameras, lifting straps, and foam attenuation material. The mass properties were adjusted based on calculations of the changes due to the masses of these installed components. The products of inertia were not measured and were assumed to be zero. The mass properties are summarized in Table 2. Note that the center of mass positions are defined relative to the spherical nose of the outer mold line and the moments of inertia are defined at the center of mass.

Table 2 Test article mass properties.

m kg	x_{cm} m	y_{cm} m	z_{cm} m	I_{xx} kg-m^2	I_{yy} kg-m^2	I_{zz} kg-m^2
98.58	-0.25704	0.00152	0.00046	11.535	7.39	7.397

V. Reconstruction Results

The drop test vehicle trajectories were reconstructed from the available measurement data using a Kalman filter tool known as the New Statistical Trajectory Estimation Program (NewSTEP) [4, 5]. The filter was configured to integrate equations of motion based on the measured IMU accelerations and rates during free fall. The process uncertainties were configured to consider the systematic errors in the IMU measurements. The GPS and weather balloon data provided corrections to the trajectory predictions based on the Kalman filter update. The trajectory estimate was smoothed using a Fraser-Potter fixed interval smoother. The filter outputs estimates of the inertial trajectory, atmosphere-relative trajectory, and aerodynamics of the test article along with the associated uncertainties.

Results of the reconstruction are shown in Figs. 10–11. The reconstructed initial altitudes, velocities, attitudes and angular rates are shown in Table 3.Figs. 10 shows the reconstructed above ground level (AGL) altitude and the planet-relative velocity magnitude. The peak velocities correspond to a Mach number of approximately 0.13. The 3σ uncertainties in position, velocity, and attitude were less than 1 m, 0.25 m/s, and 3 deg, respectively, for all four tests.

Table 3 Reconstructed initial conditions.

Drop Test	h_{agl} m	V_n m/s	V_e m/s	V_d m/s	ϕ deg	θ deg	ψ deg	ω_x deg/s	ω_y deg/s	ω_z deg/s
1	1618.04	-20.59	0.68	0.01	-99.71	-76.81	-102.38	-22.48	-3.00	0.07
2	1189.42	-3.40	-6.52	0.39	23.20	-82.23	-145.87	-7.59	-0.17	-1.79
3	1555.64	-3.41	-0.37	3.73	-129.44	-88.44	71.48	6.21	-0.21	1.36
4	1581.34	4.57	-4.41	-0.71	145.20	-85.55	125.06	3.94	1.12	-1.26

The reconstructed dynamic pressure and total angle of attack are shown in Fig. 11. Recall that the flow angles are defined in Fig. 2(c). The flow angles were computed based on the reconstructed body velocities and the winds

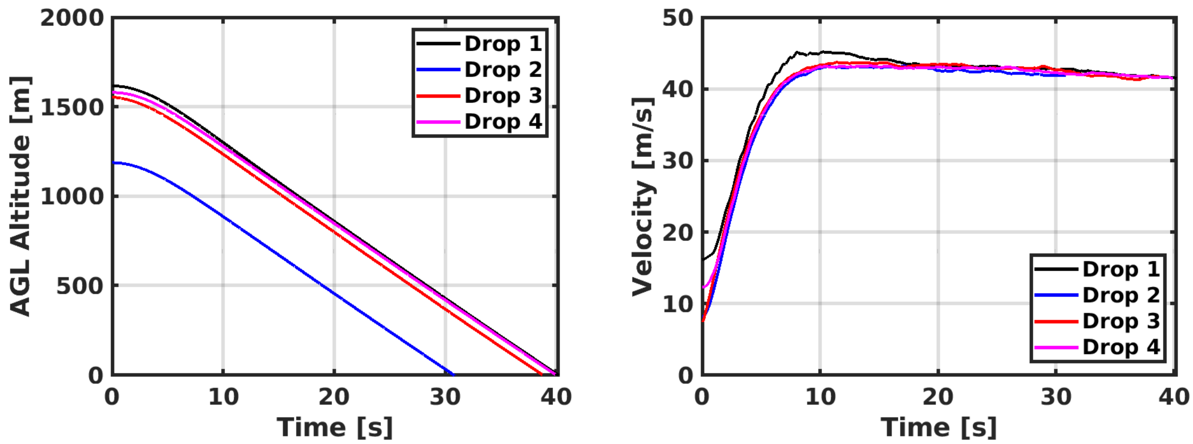

(a) AGL altitude.

(b) Velocity.

Fig. 10 Reconstructed trajectories: altitude and velocity.

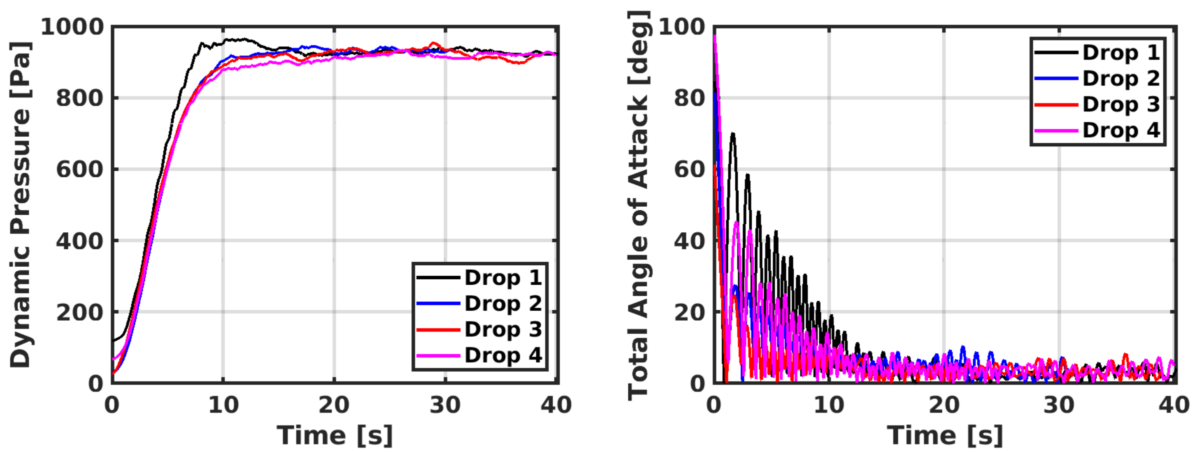

(a) Dynamic pressure.

(b) Total angle of attack.

Fig. 11 Reconstructed trajectories: dynamic pressure and total angle of attack.

measurement by the meteorological balloons. After initial transients, the amplitude of the capsule oscillation was roughly 6-8 deg. The 3σ uncertainties in dynamic pressure and total angle of attack were less than 12 Pa and 1.5 deg, respectively, for all four tests.

The conditions at impact are listed in Tables 4. Table 4 shows the reconstructed NED attitude angles and components of the angular rates and the components of the NED velocity and the velocity magnitude at the instant of ground impact. The impact velocity prediction based on nominal GRAM atmosphere, nominal aerodynamics, and perfect vertical drop initial conditions was 41.1 m/s. All four drop tests had a higher impact velocity ranging from 41.5 to 42.0 m/s. This discrepancy is likely due to a more persistent angle of attack oscillation than the simulation predictions and the unmodeled effects of helicopter rotor downwash. Angle of attack comparisons between simulation and reconstruction are shown in Sec. VI.

Table 4 Reconstructed impact conditions.

Drop Test	V_n m/s	V_e m/s	V_d m/s	ϕ deg	θ deg	ψ deg	ω_x deg/s	ω_y deg/s	ω_z deg/s
1	5.15	1.07	41.54	235.62	-86.90	154.00	-11.47	0.65	-8.34
2	2.68	0.19	41.89	-125.00	-86.44	-33.54	-17.58	5.43	-3.08
3	1.35	-0.43	41.78	-149.24	-86.28	-610.50	11.04	-19.36	-12.96
4	-2.32	1.02	41.41	-163.57	-88.20	77.80	-1.82	5.55	-14.06

An equation-error method [7] was utilized to compute estimates of the aerodynamic parameters of the test article based on data from all four tests combined in a single analysis. The uncertainty factors of the aerodynamic database were used as parameters to compute a best fit to the reconstructed aerodynamics based on the weighted sum-square residual between the reconstructed and the dispersed aerodynamics. The fits were performed on a time range from 3.5 s after drop to the time of impact to eliminate initial transient caused by low dynamic pressures and unmodeled helicopter rotor downwash. The parameters include adders and multipliers on the aerodynamic coefficients. Note that the side/normal force and pitch/yaw moment multipliers are constrained to be identical. The pre-flight aerodatabase uncertainty factors are normalized in such a way that they have a zero nominal value and a unit 3σ value. The best-fit solution parameters and associated uncertainties are listed in Table 5.

Table 5 Reconstructed aerodynamic parameters.

	C_A Multiplier	C_N Adder	C_N/C_Y Multiplier	C_Y Adder	C_m Adder	C_m/C_n Multiplier	C_n Adder
Estimate	0.1641	-0.5860	-0.6577	-0.3115	-0.3949	-0.6476	0.6854
3σ	0.0030	0.0040	0.0123	0.0267	0.0594	0.0641	0.0595

Damping coefficients were determined to be unobservable from this set of drop test data. Inclusion of the damping coefficient when solving for the aerodynamic parameters does not affect the static coefficient values or resulting reconciled trajectory. The functional form of the current damping model does not allow for any dispersion value that can replicate the observed capsule oscillations at terminal velocity conditions. The current damping model, based on forced oscillation wind tunnel data, is a roughly constant negative value for small oscillation amplitudes. A constant negative value predicts all oscillations will damp out almost completely. However, free flight testing and these full scale drop tests both show the vehicle oscillation amplitudes approach a constant amplitude between 5 and 10 degrees. There must be some mechanism adding energy to the capsule oscillations that is not captured by the current dynamic stability data. This is suspected to be from the unknown effects of helicopter downwash, higher frequency wind variations in the atmosphere, or nonlinear damping characteristics that are not being measured in a one degree-of-freedom forced oscillation pitch damping test. Assessing the sensitivity to wind modeling and investigating better low speed dynamic stability test methods are work to go.

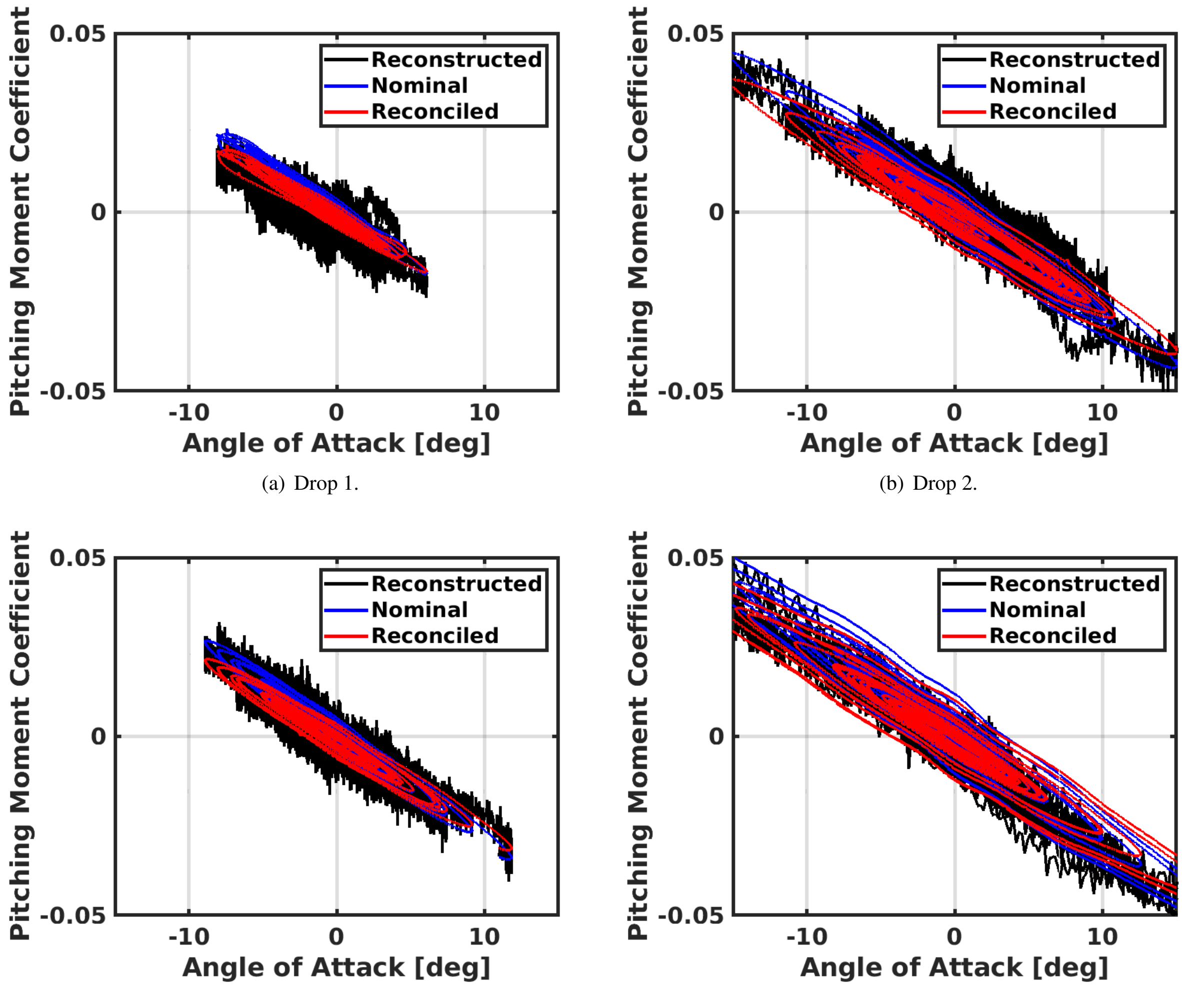

(a) Drop 1. (b) Drop 2. (c) Drop 3. (d) Drop 4.

Fig. 12 Reconstructed trajectories: pitching moment coefficient.

The reconstructed multipliers on the pitch and yaw moments indicate a lower than nominal static stability derivative. A comparison with the reconstructed pitching moment coefficient vs. angle of attack is shown in Fig. 12. The black curve shows the reconstructed values based on the measured angular rates, the blue curve shows the nominal aerodatabase evaluated along the reconstructed trajectory, and the red curve shows the best-fit dispersed aerodatabase evaluated along the reconstructed trajectory. The results show difference in slope between the reconstruction and the nominal aerodatabase. The slope difference is rectified using the best-fit dispersed aerodynamic parameters. Similar results were obtained for the yaw moment coefficient but are not shown here.

VI. Comparison with Simulation

The reconstructed trajectories were compared with flight simulations based on the Program to Optimize Simulated Trajectories II (POST2) [9]. The simulation was updated to the measured mass properties, day-of-flight atmosphere data for each drop, the as-flown initial conditions, and the reconstructed set of dispersed aerodynamic parameters. This updated simulation result is termed the *reconciled* trajectory. The reconciled trajectory altitude, velocity, and total angle of attack results are compared with the reconstruction in Figs. 13–15. The simulations consistently show a longer flight time from release to impact and a correspondingly lower terminal velocity. The simulated impact times are 0.9 to 1.3 s longer than the reconstructions. The simulations cases predict impact velocities ranging from 40.3 to 40.5 m/s whereas the reconstructed impact velocities ranged from 41.5 to 42.0 m/s.

.

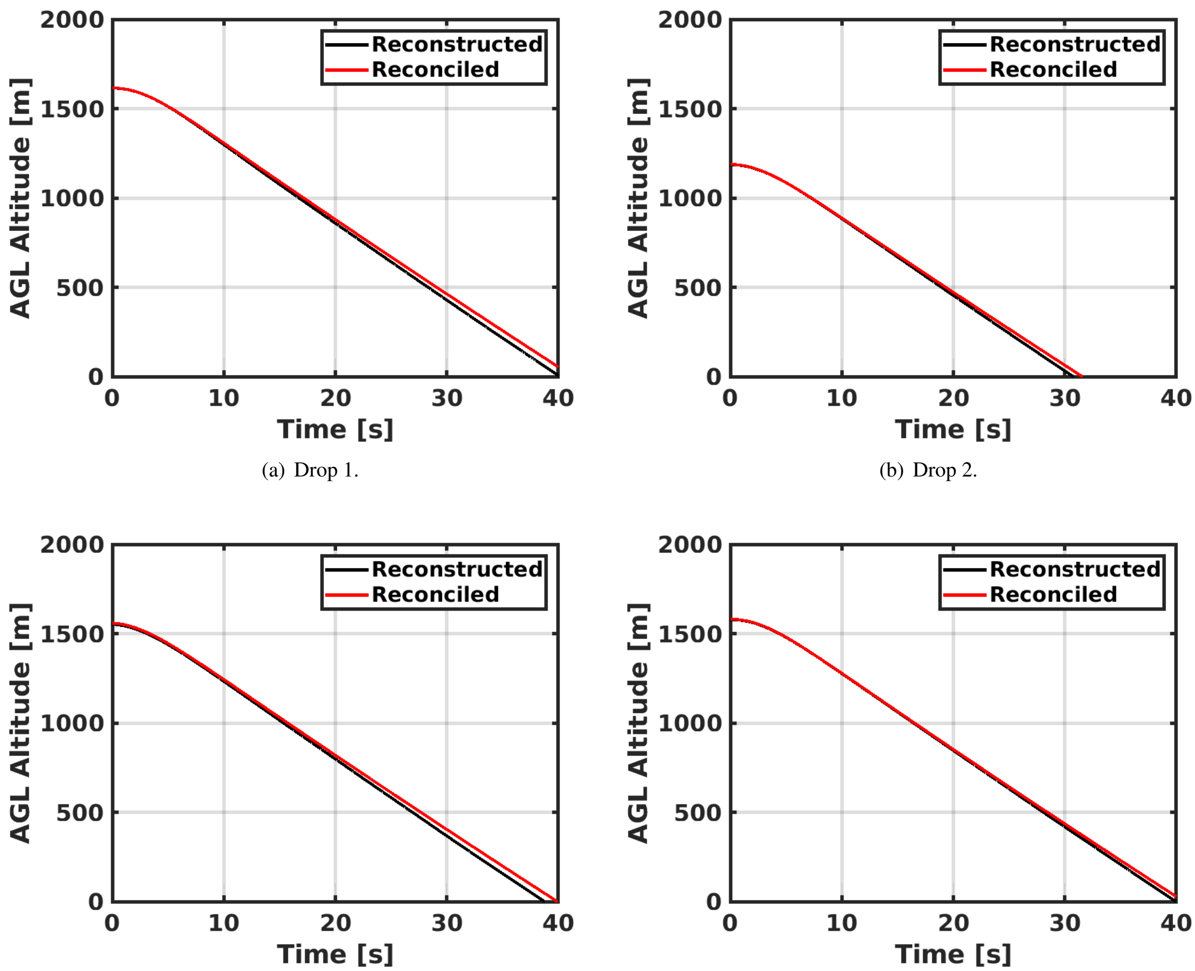

(a) Drop 1.

(b) Drop 2.

(c) Drop 3.

(d) Drop 4.

Fig. 13 Comparison with simulated trajectories: altitude.

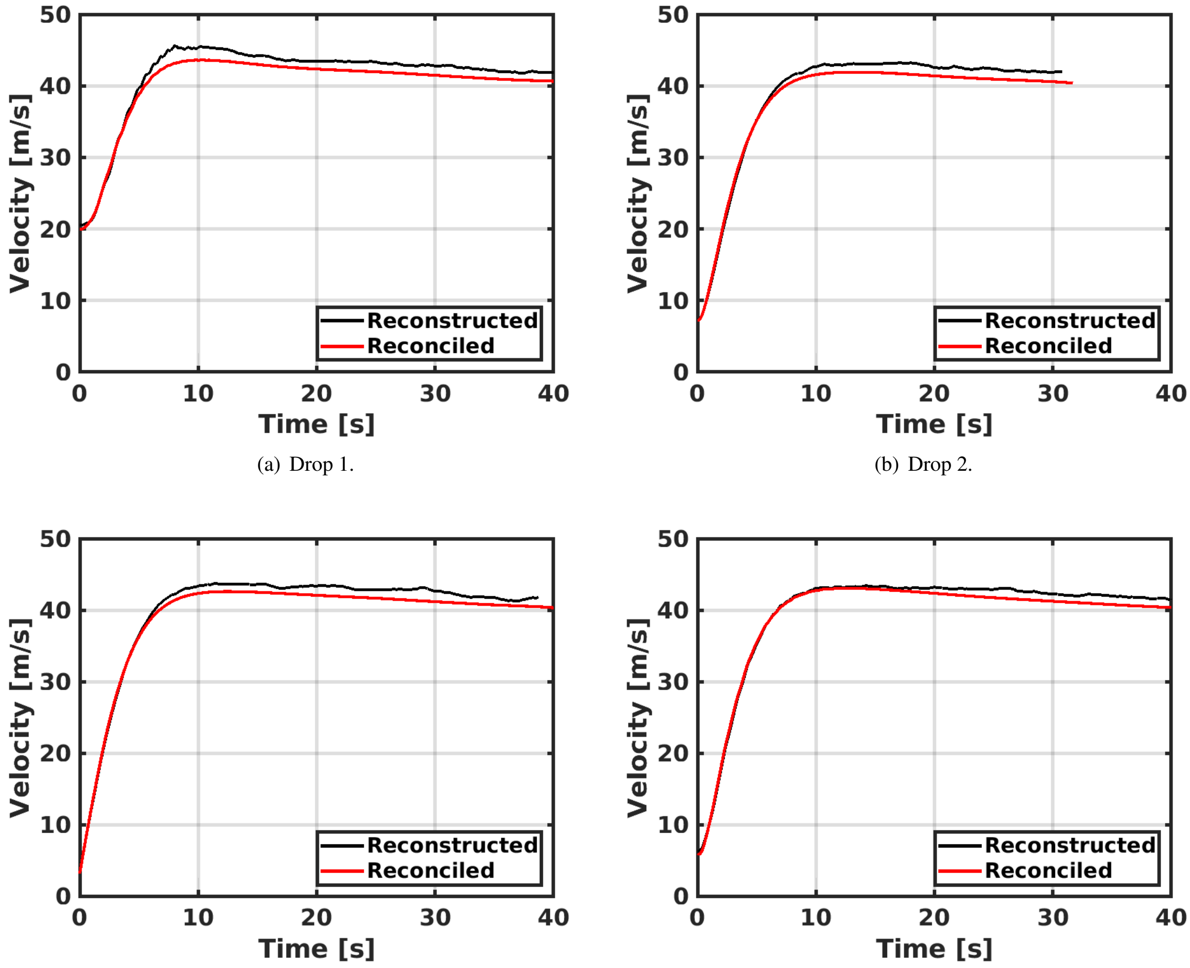

(a) Drop 1.

(b) Drop 2.

(c) Drop 3.

(d) Drop 4.

Fig. 14 Comparison with simulated trajectories: velocity.

The reconstructed trajectories show a persistent angle of attack oscillation that continues after the simulated cases have damped out. This persistent oscillation is one potential contributor to the difference in terminal velocities between reconstruction and simulation. The oscillation can be attributed to some combination of unknown low-amplitude damping characteristics of the capsule, higher frequency wind gusting that is not captured in the balloon data, or the unknown effects of helicopter rotor downwash influencing the motion of the capsule.

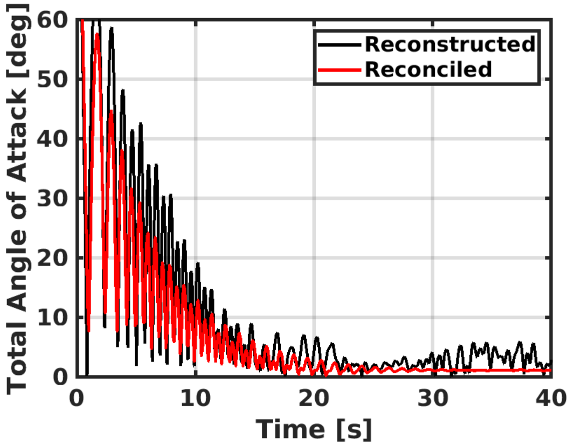

(a) Drop 1.

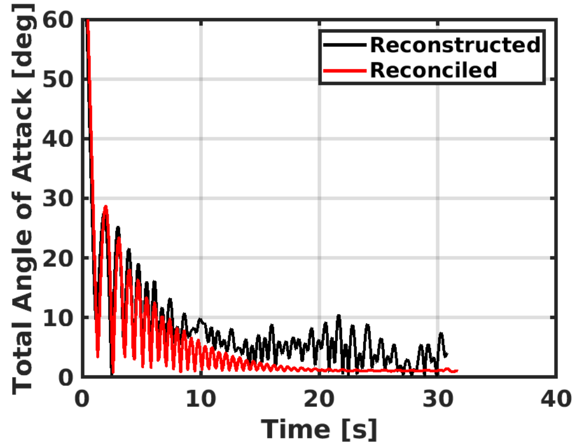

(b) Drop 2.

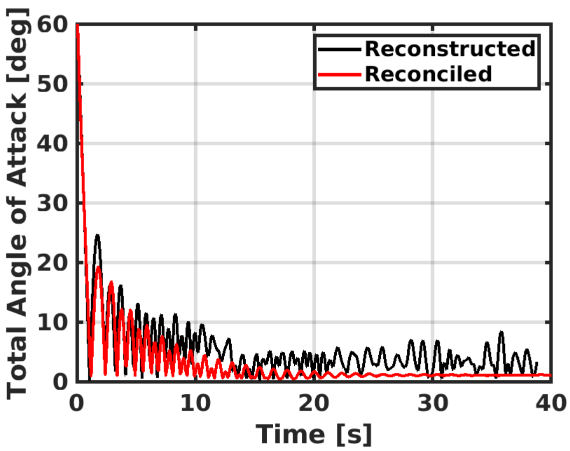

(c) Drop 3.

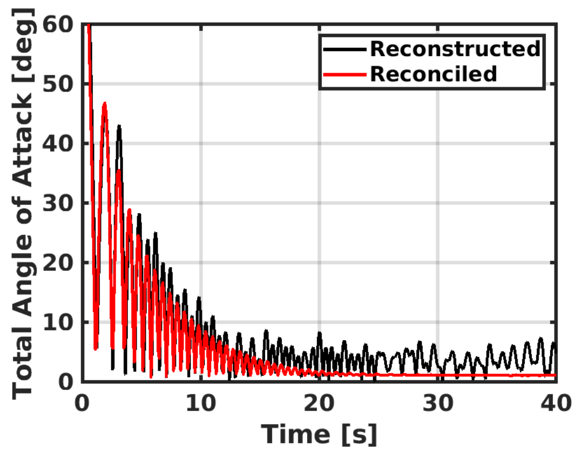

(d) Drop 4.

Fig. 15 Comparison with simulated trajectories: total angle of attack.

VII. Conclusions

Four successful helicopter drop tests of the Earth Entry System capsule were conducted. The tests were designed to collect free-flight data on the aerodynamic performance of the 52.5 deg sphere-cone capsule geometry, and secondarily to obtain soil impact data. The drop test trajectories were reconstructed from the on-board measurements using a Kalman filter/smoother. Aerodynamic parameters were extracted using an equation-error approach. The results indicate that the capsule exhibits more angular motion than predicted by trajectory simulations, including a low-amplitude persistent angle of attack oscillation that does not damp out as predicted. The cause of the of angular motion could be attributable to uncertainties in the aerodynamic damping model, high frequency wind content that was not captured in the weather balloon data, or unknown effects of helicopter rotor downwash. The results of the reconstruction will be used to inform further aerodynamic modeling of the entry capsule.

Acknowledgments

The weather balloon data were provided by the U.S. Army Dugway Meteorological Office. The test article mass property measurements and calculations were performed by the Systems Integration and Test Branch at the NASA Langley Research Center.

References

[1] Muirhead, B. K., Nicholas, A. K., Umland, J., Sutherland, O., and Vijendran, S., "Mars Sample Return Campaign Concept Status," *Acta Astronautica*, Vol. 176, 2020, pp. 131–138. https://doi.org/10.1016/j.actaastro.2020.06.026

[2] Deshmukh, R., and Manwell, M., "Flight Mechanics Modeling and Simulation of The Earth Entry System," 21st International Planetary Probe Workshop, Williamsburg, VA, June 2024.

[3] White, P. W. and Hoffman, J., "Earth Global Reference Atmospheric Model (Earth-GRAM): User Guide," NASA/TM-20210022157, September 2021.

[4] Karlgaard, C., Tartabini, P., Blanchard, R., Kirsch, M., and Toniolo, M., "Hyper-X Post-Flight Trajectory Reconstruction," *Journal of Spacecraft and Rockets*, Vol. 43, No. 1, 2006, pp. 105-115. https://doi.org/10.2514/1.12733

[5] Karlgaard, C., Beck, R., Derry, S., Brandon, J., Starr, B., Tartabini, P., and Olds, A., "Ares I-X Trajectory Reconstruction: Methodology and Results," *Journal of Spacecraft and Rockets*, Vol. 50, No. 3, 2013, pp. 641-661. https://doi.org/10.2514/1.A32345

[6] Dutta, S., Guecha-Ahumada, N. G., Andreini, M., J., and Karlgaard, C. D., "Helicopter Drop Test and Results of the DAVINCI Descent Sphere," AIAA Aerodynamic Decelerator Systems Conference, AIAA Paper 2024-XXXX, July 2024.

[7] Morelli, E. A. and Klein, V., *Aircraft System Identification: Theory and Practice*, Second Edition, Sunflyte Enterprises, Williamsburg, VA, 2016.

[8] Owens, B., Weinstein, R., Giles, I., and Schoenenberger, M., "Aerodynamic Stability Characterization of the Mars Sample Return (MSR) Earth Entry System (EES) in the Transonic Dynamics Tunnel," Invited Presentation, AIAA SciTech Forum and Exposition, Orlando, FL, January 2024. https://ntrs.nasa.gov/citations/20230018603

[9] Williams, R. A., Lugo, R. A., Marsh, S. M., Hoffman, J. A., Shidner, J., and Aguirre, J. T., "Enabling Thread Safety and Parallelism in the Program to Optimize Simulated Trajectories II," AIAA Paper 2023-0148, January 2023. https://doi.org/10.2514/6.2023-0148